Applied Catalysis A: General 516 (2016) 135–143

Contents lists available at ScienceDirect

Applied Catalysis A: General

journal homepage: www.elsevier.com/locate/apcata

n-Heptane isomerization over mesostructured silica nanoparticles (MSN): Dissociative-adsorption of molecular hydrogen on Pt and Mo sites

N.A.A. Fatah[a], S. Triwahyono[b,*], A.A. Jalil[a,c], A. Ahmad[a,c], T.A.T. Abdullah[a,c]

[a] Department of Chemical Engineering, Faculty of Chemical and Energy Engineering, Universiti Teknologi Malaysia, 81310 UTM Johor Bahru, Johor, Malaysia
[b] Department of Chemistry, Faculty of Science, Universiti Teknologi Malaysia, 81310 UTM Johor Bahru, Johor, Malaysia
[c] Centre of Hydrogen Energy, Institute of Future Energy, Universiti Teknologi Malaysia, 81310 UTM Johor Bahru, Johor, Malaysia

ARTICLE INFO

Article history:
Received 24 October 2015
Received in revised form 19 February 2016
Accepted 25 February 2016
Available online 27 February 2016

Keywords:
n-Heptane isomerization
Molybdenum
Platinum
Mesostructured silica nanoparticles
Hydrogen dissociation

ABSTRACT

Mesostructured silica nanoparticles (MSN) were mixed physically with Pt and MoO_3 to prepare Pt/MSN and MoO_3/MSN for *n*-heptane isomerization. The XRD, N_2 physisorption and 2,6-lutidine-adsorbed infrared (IR) spectroscopy studies showed that the introduction of Pt did not change the properties of MSN much due to lack of-interaction between Pt and the silicate framework of the MSN. However, MoO_3 significantly altered the pore distribution, surface area and acidity of MSN. 2,6-Lutidine adsorbed IR showed the formation of new doublet absorbance bands at 1638 and 1631 cm^{-1} corresponding to the presence of permanent acidic Brønsted sites. The isomerization of *n*-heptane distinguished the low catalytic activity of MSN, MoO_3, and Pt/MSN in the presence of either hydrogen or nitrogen gas. High activity of *n*-heptane isomerization was observed on MoO_3/MSN in the presence of hydrogen with yield of mono- and di-branched isoheptane reached 36.6 and 6.8%, respectively. No deactivation was observed on MoO_3/MSN after 100 h of the reaction. ESR and IR studies indicated that the high activity and stability of MoO_3/MSN could be attributed to the dissociative-adsorption of molecular hydrogen to form atomic hydrogen, which subsequently formed active $(MoO_x)^-(H_y)^+$. Although Pt sites have better ability to interact with hydrogen than Mo sites, the electrically neutral charge of the silicate framework was not able to form active protonic acid sites on the Pt/MSN, which only yield less than 1% isoheptane. It is plausible that the interaction of Pt/MSN and molecular hydrogen formed Pt-H which was not active in *n*-heptane isomerization.

1. Introduction

In the petrochemical industry, hydroisomerization is a key reaction for the production of high quality liquid fuels. Nowadays, the focus has shifted to light straight–chain C_5 —C_8 paraffins as feeds for hydroisomerization. The branched isomers of C_5—C_8 paraffins possess a higher octane number compared to the corresponding linear paraffins (C_7) [1–3]. It is well known that the isomerization reaction proceeds through consecutive branching reactions over bifunctional metal-acid catalysts. The isomerization occurs at the acid sites of the bifunctional catalyst, while the metal site provides hydrogenation-dehydrogenation capability [4,5]. Previously, many studies have focused on various type of zeolite catalyst for isomerization since conventional catalysts such as chlorided Pt alumina lead to corrosion and environmental problems. It has been reported that zeolite Pt/mordenite catalyst was catalytically active for *n*-C_5 isomerization due to its high acidity; however, it exhibited less selectivity when dealing with longer chain paraffins such as *n*-C_6 and *n*-C_7 [6]. The limitation of zeolite catalyst for longer chain alkanes has led to the further development of isomerization catalyst with both mesoporosity and balanced acidity properties.

Recently, the development of mesostructured silica nanoparticles (MSN) with a highly ordered mesostructure, high surface area, large pore volume and well-defined pore size has attracted a lot of attention. MSN has been successfully applied in many different applications such as CO_2 reforming of CH_4 [7], methanation of CO_2 [8], drug delivery [9] and adsorption [10]. The tuneable pore size of MSN and high surface area offer an opportunity to design an isomerization catalyst for linear chain alkane longer than *n*-C_5. However, the MSN requires modification to provide acidic property since it consists of silica framework with no Brønsted acid sites [11]. In

* Corresponding author.
E-mail addresses: sugeng@utm.my, sugeng@ibnusina.utm.my (S. Triwahyono).

http://dx.doi.org/10.1016/j.apcata.2016.02.026
0926-860X/

order to overcome this drawback, the loading of metal oxide could be useful to improve the mesostructured acidic property.

Among the metal oxide catalysts, MoO_3 has been extensively studied due to its potential in alkane isomerization and environmentally friendly properties as compared to mineral acids such as HF and H_2SO_4. Many works have been devoted to MoO_3-related catalysts and discussed in several reviews. In recent studies, Sakagami et al. reported that the catalytic activity of Pt/MoO_3 catalyst was greatly affected by its surface area [12]. The improvement in the Pt/MoO_3 surface area due to the slow reduction rate of H_2 flow gave the MoO_x with the highest *n*-heptane isomerization activity. Besides, our group has also reported on the formation of acidic Brønsted $(MoO_x)^-(H_y)^+$ over Pt/MoO_3 for cumene cracking [13]. It was evidenced by XRD and 2,6-lutidine IR spectroscopy that the presence of Pt was essential in the formation of the active site. In fact, no $(MoO_x)^-(H_y)^+$ or protonic acid sites were observed on Pt-free MoO_3.

Indeed, although there are several reports have been published on MoO_x supported SiO_2 material for short alkane isomerization, the presence of noble metal still dispensable in these type of catalysts. Early study by Gallo et al. reported that the *n*-heptane isomerization activity of MoO_3-carbon modified supported on silica carbide was influenced by its total activation pressure. A selectivity of 12.8% *di*-branched isomers was obtained over the MoO_3/SiC after 24 h activation at with 40 bar total activation pressure [14]. On the other hands, Matsuda et al. have reported that *n*-heptane isomerization over Pt/MoO_3-SiO_2 can be controlled by the formation of MoO_xH_y, yielded from the reduction of MoO_3 along with its number of acid sites. The Pt/MoO_3-SiO_2 catalyst with 80 wt.% of MoO_3 gave 17.3% selectivity of di-branched isomers at 350 °C [15].

In this present work, MSN was used as MoO_3 support and *n*-heptane isomerization was chosen as a model reaction. The role of the MSN as a silica framework with weak Lewis acid property in facilitating the formation of (MoO_x)-$(H_y)^+$ by trapping electron was emphasized in correlation with its catalytic activity. The presence of interparticles textural porosity, which contributes to a high surface area and large pore diameter of MSN, promises a new design of catalyst with highly dispersed and accessible active sites, leadings to selective towards mono- and *di*-branced isomer products. In addition, the physico-chemical properties and catalytic activity of MoO_3/MSN were compared with Pt/MSN, since Pt is well known as an active noble metal for alkane isomerization.

2. Experimental

2.1. Catalyst preparation

Mesostructured silica nanoparticles (MSN) were prepared according to the procedure in literature [10]. In brief, the cetyltrimethylammonium bromide (CTAB, Merck) surfactant, ethylene glycol (EG, Merck) and ammonium hydroxide solution (NH_4OH, QRec) were dissolved in 700 ml of water with a mol composition of 0.0032:0.2:0.2:0.1, respectively. The resulting mixture was stirred for 30 min with heating to obtain a clear and homogeneous solution. Then 1.2 mmol of tetraethoxysilane (TEOS, Merck) and 1 mmol 3-aminopropyl triethoxysilane (APTES, Merck) were gradually added under vigorous stirring for another 2 h to give a white suspension solution. The mixture was subsequently collected by centrifugation and then extensively washed with deionized water. The synthesized MSN were dried at 110 °C overnight and calcined at 550 °C for 3 h to remove the surfactant.

MoO_3 was prepared by calcination of H_2MoO_4 at 550 °C for 3 h. The MoO_3/MSN catalyst was prepared by mixing the MoO_3 and MSN powder in a planetary ball mill with an agate container having 300 cm^3 volume and six 20 mm diameter-agate ball with a weight of approximately 11 g each. After 1 h milled, the mixture was calcined in air at 550 °C. The Pt/MSN was prepared by physical mixing of MSN with 0.5 wt.% Pt black, using similar method as MoO_3/MSN preparation followed by calcination at 550 °C for 3 h in air.

2.2. Characterization of catalyst

The crystalline structure of catalysts was determined with X-ray diffractometer (Bruker Advance D8, 40 kV, 40 mA) using Cu Kα (λ = 1.5418Å) radiation in the range of $2\theta = 20 - 60°$. The nitrogen physisorption analysis of the catalysts was carried out by using a Beckman Coulter physisorption equipment, model SA 3100. Prior to the measurement, the catalyst was outgassed at 573 K for 1 h. Then, adsorption of nitrogen was carried out at −196 °C. Surface area, pore size distributions and pore volumes were determined from the sorption isotherms using a non-local density functional theory (NLDFT) method.

Fourier Transform Infra-Red (IR) measurements were carried out using Agilent Carry 640 FTIR Spectrometer. Before analysis, the catalysts were activated according to the method described in the literature [13]. In brief, a self-supported wafer was placed in an in situ stainless steel IR cell with CaF_2 windows and activated at 400 °C for 1 h. For 2,6-lutidine adsorption, the activated catalysts were exposed to 4 Torr of 2,6-lutidine at room temperature for 15 min, followed by outgassing at 100 °C. For the study of the interaction hydrogen and the surface of the catalysts, 2,6-lutidine pre-adsorbed catalyst was exposed to 100 Torr of hydrogen at room temperature followed by stepwise heating from room temperature to 200 °C in 50 °C increments. All spectra were recorded at room temperature.

UV diffuse reflectance spectrum (UV-DRS) was recorded in air at room temperature over a range of wavelengths from 200 to 800 nm with an Agilent Cary 60 UV–vis with PIKE Diffuse reflectance accessory. In this experiment, pure magnesium oxide was used as a reference [16].

A JEOL JES-FA100 ESR spectrometer was used to observe the formation of unpaired electrons during in vacuo heating and to observe the interaction of unpaired electrons with electrons from molecular hydrogen. The catalyst was outgassed at 400 °C for 1 h followed by introduction of 100 Torr of gaseous hydrogen at room temperature. Then, the catalyst was heated from 50 °C to 200 °C in 50 °C increments. All signals were recorded at room temperature.

Temperature programmed reduction (TPR) analysis was carried out for determining the reduction temperature of the different metallic phases of the catalysts. The analysis was conducted at atmospheric pressure by using a Micromeritics Chemisorb 2720 Pulse Chemisorption in 10% H_2/Ar at a heating rate of 10 °C min^{-1}.

2.3. Isomerization of n-heptane

The isomerization of *n*-heptane was conducted in a microcatalytic pulse reactor at temperature range of 100–350 °C. Prior to the reaction, 0.3 g of catalyst was activated in an oxygen stream (F_{Oxygen} = 100 ml/min) at 400 °C for 1 h, followed by hydrogen stream ($F_{Hydrogen}$ = 100 ml/min) at 400 °C for 3 h. A dose of *n*-heptane (34 μmol) was passed over the activated catalyst, and the products were trapped at −196 °C before flash-evaporation into an online 6090 N Agilent Gas Chromatograph equipped with HP-5Capillary Column and an FID/MS detector. The selectivity (S_i), yield to particular product and conversion of *n*-heptane ($X_{n\text{-heptane}}$) were calculated according to Eqs. (1)–(3), respectively.

$$Si(\%) = \frac{Ci}{\sum Ci - Cres\_reactant} \times 100\% \quad (1)$$

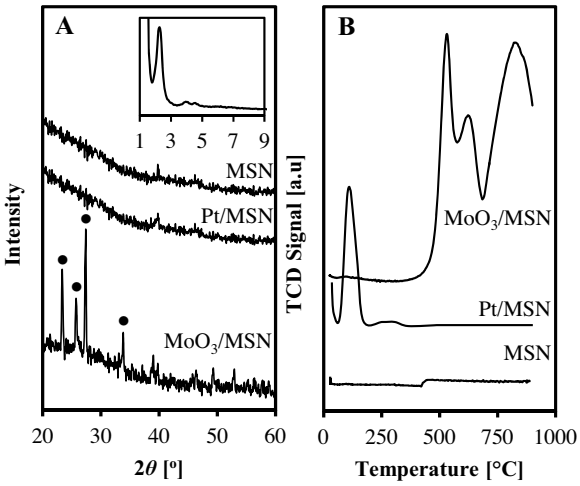

Fig. 1. (A) Wide angle XRD pattern of MSN and MSN supported catalysts (B) FTIR spectra of (a) MSN, (b) Pt/MSN and (c) MoO_3/MSN.

$$Xreactant = \frac{\sum C_i - Cres\_reactant}{\sum C_i} \quad (2)$$

$$Y_i = \frac{Xreactant \times Si}{100} \quad (3)$$

where C_i and $C_{res\_reactant}$ are mole number of particular compound and for residual reactant which was calculated based on the Scott hydrocarbon calibration standard gas (Air Liquide America Specialty Gases LLC). While, the specific rate conversion data was obtained by multiplication of the differential conversion data and rate constant (k). The rate constant was determined by the molar concentration of the reactant divided by mass of the catalyst per unit time with the assumption that the retention time for reactant in the catalyst bed was negligibly small.

3. Results and discussion

3.1. Structural properties of catalysts

Fig. 1A shows the wide-angle XRD pattern of MSN, Pt/MSN and MoO_3/MSN catalysts in the range of $2\theta = 20 - 60^\circ$. The metallic crystallite peak was not observed for MSN, indicating that the sample has no metallic particles. No peaks corresponding to the presence of Pt crystal were observed in Pt/MSN. This may be due to the high dispersion or diminutive amount of Pt, which was beyond the detection limit of XRD. For MoO_3/MSN, the presence of MoO_3 crystallite can be observed with the presence of several sharp diffraction peaks at $2\theta = 23.3^\circ$, 25.7°, 27.4° and 33.7°, which correspond to the crystalline orthorhombic phase of MoO_3 [17]. The inset figure shows the low-angle XRD pattern of parent MSN, showing the presence of an ordered hexagonal structure of the MSN. The ordered hexagonal structure did not change much with the introduction of Pt or MoO_3. A similar phenomenon was observed for alumina-loaded SBA-15 obtained by the solid state grinding method, where the mesostructure of the support composite was still retained [18].

H_2-TPR profiles of MSN, Pt/MSN and MoO_3/MSN are shown in Fig. 1(B). The MSN did not show any reduction peaks, while a single reduction peak was observed in the temperature range of 50–264 °C for Pt/MSN due to the reduction of Pt^{2+} cations. This result was similar to the H_2-TPR of Pt/Si-MCM-41 reported by Shen et al., where only a single peak was observed for low loading of Pt [19]. However, the increase in the Pt loading on Si-MCM-41 formed two different TPR peaks due to the agglomeration of Pt on the surface. Since a single peak was observed for Pt/MSN, it can be concluded that the Pt occurrence on MSN was only in the single form of PtO_2 [20].

The TPR profile of MoO_3/MSN showed two main reduction peaks. A sharp peak was observed at 537 °C, which corresponds to the reduction of MoO_3 to MoO_2, while the other peak at 827 °C was associated with the reduction of MoO_2 to Mo [21]. A minor peak at the edge of the first major peak was observed at 630 °C, which corresponds to Mo_4O_{11} formed by the reduction of MoO_3 [22]. These results indicated that at least three types of molybdenum species are present in the MoO_3/MSN catalyst. Based on H_2-TPR study of bulk MoO_3 by Arnoldy et al., peaks corresponding to the reduction of MoO_3 to MoO_2 and MoO_2 to Mo were observed at 724 and 767 °C, respectively [23]. The shift of the reduction peaks for MoO_3/MSN to a lower temperature compared to the bulk MoO_3, suggested that the MoO_3 was highly dispersed on the surface of the MSN.

FT-IR measurement was performed to distinguish the structural differences of the catalysts. In Fig. 2A, the FTIR spectrum of MSN in the range of 1600–400 cm^{-1} demonstrated the absorbance bands corresponding to Si—O—Si bending (458 cm^{-1}), Si—O—Si symmetric stretching (792 cm^{-1}), external Si—OH groups (960 cm^{-1}), and Si—O—Si asymmetric stretching (1080 cm^{-1}) [9,24]. The spectrum of the Pt/MSN was almost the same as that of the MSN, indicating that MSN still retained its silicate framework without major changes after Pt loading. Meanwhile, three new bands were observed for MoO_3/MSN spectra, which attributed to Mo—O (586 cm^{-1}), Mo—O—Mo (864 cm^{-1}) and Mo = O stretching mode (990 cm^{-1}) [25]. Besides, a small band was observed at 820 cm^{-1}, which was attributed to vibrations of oxygen atoms connected to two orthorhombic MoO_3 structures [26], whereas; the Si—O—Mo band could not be clearly distinguished due to the overlapping with the Si—O—Si absorbance band at 458 cm^{-1}.

However, the interaction between MoO_3 and MSN could be inferred from the changes in the lattice structure of the MSN. The lattice stretching region of MSN-based catalysts can be characterized by two main broad peak at 1862 and 1627 cm^{-1} along with a shoulder peak at 1974 cm^{-1} (Fig. 2B) [27]. MSN and Pt/MSN showed similar patterns of IR spectra, suggesting that the Pt did not interact with the silicate framework. Meanwhile, the addition of MoO_3 has constricted the peaks at 1862 and 1627 cm^{-1} and intensified the peak at 1627 cm^{-1}. In addition, small new peaks were formed at about 1658 cm^{-1}. Thus, it can be concluded that the MoO_3 has formed an interaction with the silicate framework of MSN as observed by the changes occurred in the lattice stretching region.

Fig. 2C shows the IR spectra of the hydroxyl group region, in which all catalysts possess three absorbance bands at 3737, 3678 and 3655 cm^{-1} corresponding to the terminal Si-OH group, hydrogen bridges (Si—OH···HO—Si) in the mesoporous silica wall, and OH stretching bands respectively [28]. No changes were observed in the hydroxyl region of MSN after the incorporation of Pt. This is might be due to no interaction between Pt and silicate framework. However, the addition of MoO_3 into MSN has additionally formed three new absorbance bands at 3600, 3569 and 3520 cm^{-1} and intensified the bands at 3678 and 3655 cm^{-1}. The bands at 3600 and 3569 cm^{-1} were assigned to the stretching of the structural environment OH group due to the presence of Mo, which interacts with the lattice structure of MSN, while the latter band at 3520 cm^{-1} was attributed to bridging hydroxyl groups that were perturbed by H-bond interaction within the mesoporous network [29,30].

Fig. 2(D) shows the UV diffuse reflectance spectra of all catalysts in the range of 200–800 nm. No significant peak was observed for the MSN support. The MoO_3/MSN shows a broad adsorption band in the range of 200–360 nm, corresponding to tetrahedrally coordinated Mo(VI) and a small shoulder peak in the range of 360–415 nm which can be recognized as octahedrally coordinated Mo(VI) [31]. According to the previous study, the tetrahedrally coordinated Mo(VI) species suggests the presence of strong Mo-support interaction caused by calcination while the octahedrally coordinated Mo(VI) species could be associated to a low Mo-

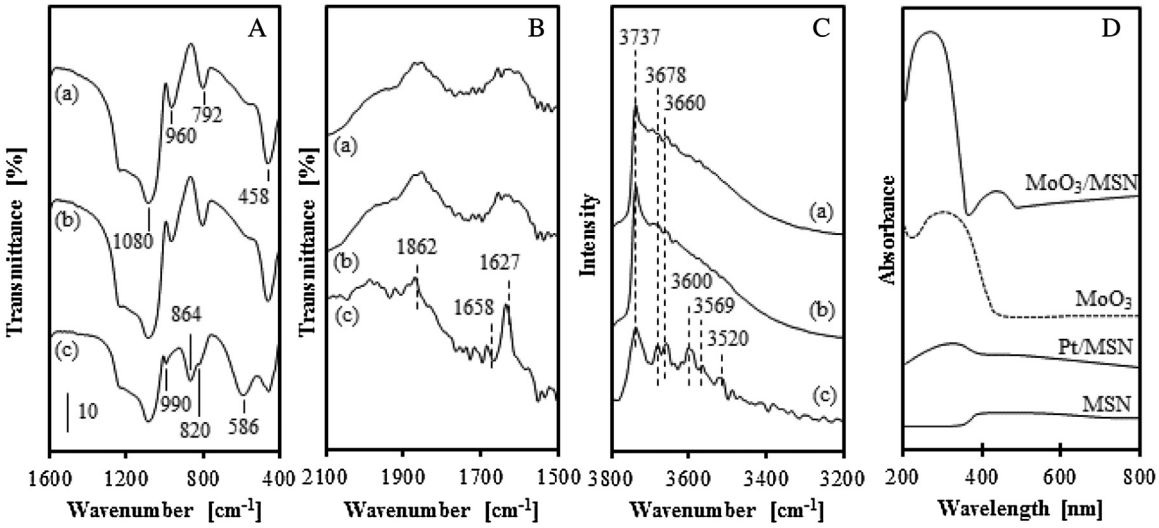

Fig. 2. (A) and (B) IR KBr spectra and (C) activated OH region of (a) MSN, (b) Pt/MSN and (c) MoO_3/MSN.

support interaction [32]. However, in this study it is plausible that the tetrahedrally coordinated Mo(VI) species formed an interaction at surface of MSN, since peak intensity of external Si—OH (960 cm^{-1}) for MoO_3/MSN was decreased compared to MSN support [33]. These result was in agreement with the changes occurred in the lattice structure of MSN after incorporation of MoO_3, as illustrated in Fig. 2B.

Fig. 3 shows the nitrogen adsorption–desorption isotherms and pore size distribution of catalysts. The MSN and Pt/MSN demonstrate a type IV isotherm with a H1 hysteresis loop, corresponding to mesoporous materials with highly uniform cylindrical pores [34,35]. Two up-steps can be observed at $P/P_{\bigcirc} = 0.3$ and 0.9, indicating the capillary condensation of nitrogen in the intraparticle and interparticle voids, respectively. It was seen that a narrow peak centered at a pore width of 3.77 nm of the MSN was significantly decreased by the introduction of Pt, accompanied by the appearance of several larger pores centered at 4.72 and 16.09 nm. This may indicate that Pt partially clogged the pores of MSN and simultaneously formed interparticle void on the surface, as evidenced by the increase of the adsorption peak at $P/P_o = 0.9$. With regard to the significant changes in the pore size distribution due to the introduction of Pt, the specific surface area and average pore diameter of MSN decreased from 1080 to 1078 m^2/g and from 3.78 to 3.53 nm, respectively.

The MoO_3/MSN also exhibited a type IV isotherm with H1 hysteresis loop. The introduction of MoO_3 decreased the intraparticle and interparticle voids as demonstrated by the reduction of up-steps intensity at both $P/P_{\bigcirc} = 0.3$ and 0.9. This changed the surface area and average pore diameter to 486 m^2/g and 4.89 nm, respectively. Although the introduction of MoO_3 markedly clogged the pores of MSN centered at 3.77 nm, the presence of MoO_3 formed new larger pores centered at pore widths of 4.25, 10.13 and 16.68 nm.

3.2. Acidic properties of catalysts

2,6-Lutidine probe molecule was used to study the acidity of catalysts due to its ability to distinguish between Brønsted and Lewis acid sites and to discriminate the variable strength of acidic centers [36]. Fig. 4A shows the IR spectra of 2,6-lutidine adsorbed on the activated MSN, Pt/MSN and MoO_3/MSN in the region of 1680–1560 cm^{-1}. The MSN showed a doublet band at 1604 and 1583 cm^{-1} corresponding to the 2,6-lutidinium ions adsorbed on the Lewis acidic center, originates from the presence of electron pair acceptor sites from Si—OH groups [11]. It was observed that the doublet band corresponding to the Lewis acidic center did not change much upon the introduction of Pt into MSN. Similarly, the introduction of MoO_3 into MSN did not change the intensity of the Lewis acid sites but generated new doublet bands at 1643 and 1628 cm^{-1}. These absorbance bands are associated with 8a and 8b of lutidinium cations on the hydroxyl group (—OH) defect structure of MoO_3 and protonated 2,6-lutidine adsorbed on Brønsted acid sites, which formed as Brønsted (Mo-OH) [37]. However, almost no Brønsted acid sites were observed for MSN and Pt/MSN due to the electrically neutral framework of MSN.

The distribution of the acidic sites as a function of outgassing temperature is illustrated in Fig. 4B. The 2,6-lutidine was adsorbed on the activated catalyst and outgassed at room temperature, 50, 100, 150 and 200 °C for 30 min, respectively. All catalysts exhibited a strong interaction between acidic sites and 2,6-lutidine at room temperature, which were significantly retained in the outgassing at and below 100 °C. At higher outgassing temperature, the intensity of the Lewis acid sites of MSN decreased markedly, showing the presence of a large number of weak and a small number of moderate-to-strong ones. However, Pt/MSN retained the 2,6-lutidine at and above 150 °C. This result suggested that Pt/MSN consists of stronger Lewis acid sites than MSN due to the interaction between 2,6-lutidine and platinum crystallites, which known as electron acceptor, to acts as a Lewis acid site [38]. The distribution of Lewis acid sites for MoO_3/MSN was similar to that of MSN but a moderate change was observed at and above 150 °C. Thus, it can be inferred that the MoO_3/MSN possessed a moderate-to-strong Lewis acid sites distribution. In addition to the Lewis acid sites, MoO_3/MSN also possessed several moderate and strong permanent Brønsted acid sites in which the bands at 1643 and 1628 cm^{-1} were decreased gradually as the outgassing temperature increased up to 200 °C.

3.3. Catalytic performance

Table 1 and Fig. 5 illustrate the catalytic activity and product distribution of MSN type catalysts in the isomerization of *n*-heptane in the temperature range of 100–350 °C. In general, a low yield of *mono*-branched isomers was obtained for MSN and Pt/MSN for all reaction temperatures under hydrogen or nitrogen carrier gas. No *di*-branched isomer products were detected for these catalysts. For MSN, the C_1 —C_4 cracking products started to be observed at 250 °C and increased with the reaction temperature, showing that

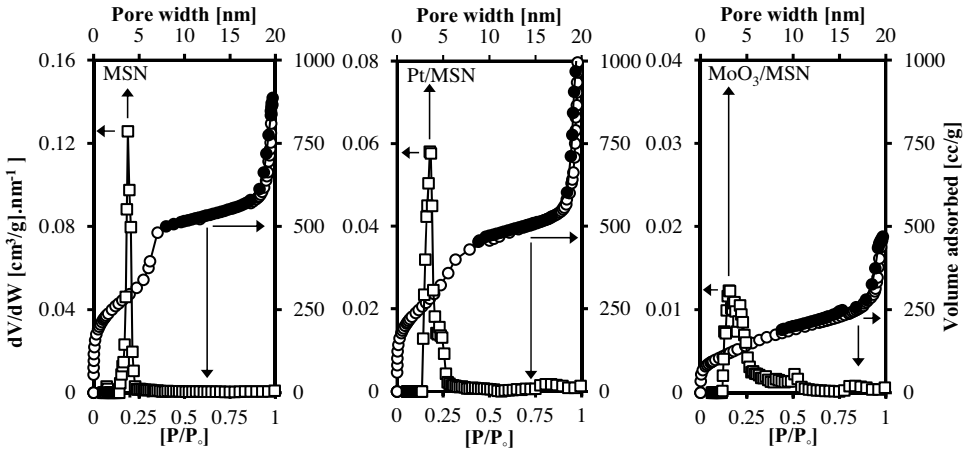

Fig. 3. N_2 adsorption (white-circle symbol)—desorption (black-circle symbol) isotherms and NLDFT pore size distribution (white-square symbol) of MSN, Pt/MSN and MoO_3/MSN catalysts.

Table 1
Product distributions of *n*-heptane isomerization in the presence of hydrogen.

	Reaction temperature [°C]					
	100	150	200	250	300	350
MSN						
Rate of conversion (10^{-9} mol/m^{2}s)	0.03	0.03	0.04	0.06	0.09	0.24
Selectivity of isomers (%)						
mono-branched	100	100	100	91.7	64.6	49
di-branched	0	0	0	0	0	0
Selectivity of cracking products (%)						
C_1—C_2	0	0	0	8.3	16.2	39.6
C_3—C_4	0	0	0	0	19.2	11.4
C_5—C_6	0	0	0	0	0	0
Yield of *di*-branched	0	0	0	0	0	0
Yield of *mono*-branched	0.1	0.19	0.21	0.17	0.17	0.37
Bulk MoO3						
Rate of conversion (10^{-9} mol/m^{2}s)	2.3	5.9	7.2	7.3	8.1	27.6
Selectivity of isomers (%)						
mono-branched	0	0	3.6	4.8	0.9	2
di-branched	0	0	0	0	0.01	0.02
Selectivity of cracking products (%)						
C_1—C_2	100	100	94.3	85.8	80.5	17.5
C_3—C_4	0	0	0	0	0	0
C_5—C_6	0	0	2.1	9.3	18.5	80.4
Yield of *di*-branched	0	0	0	0	0.01	0.01
Yield of *mono*-branched	0	0	0.4	0.6	0.13	0.94
Pt/MSN						
Rate of conversion (10^{-9} mol/m^{2}s)	0.03	0.03	0.07	0.21	0.47	0.80
Selectivity of isomers (%)						
mono-branched	100	100	64.9	24.7	9.6	6.3
di-branched	0	0	0	0	0	0
Selectivity of cracking products (%)						
C_1C_2	0	0	35.1	75.3	84.6	89.9
C_3—C_4	0	0	0	0	3.2	2.5
C_5—C_6	0	0	0	0	2.6	1.3
Yield of *di*-branched	0	0	0	0	0	0
Yield of *mono*-branched	0.1	0.1	0.13	0.17	0.14	0.16
MoO3/MSN						
Rate of conversion (10^{-9} mol/m^{2}s)	0.70	2.82	5.63	14.07	26.74	31.66 (29.8)[a]
Selectivity of isomers (%)						
mono-branched	0	0	0	0	87.9	81.3 (78.6)[a]
di-branched	0	0	0	0	6.4	15.2 (13.9)[a]
Selectivity of cracking products (%)						
C_1—C_2	0	0	0	0	0	0 (0)[a]
C_3—C_4	0	26.6	5.7	2.5	3.9	1.1 (3.5)[a]
C_5—C_6	100	73.4	94.3	97.5	1.8	2.4 (4)[a]
Yield of *di*-branched	0	0	0	0	2.4	6.8 (5.4)[a]
Yield of *mono*-branched	0	0	0	0	33.4	36.6 (25.6)[a]

The pulse reaction was carried out under H_2 gas (100 ml/min). Ten pulses were measured at each reaction temperature and the data were taken from the average of the sixth, seventh and eighth pulses.

[a] ( ) is the continuous flow reaction data at 350 °C and *n*-heptane/H_2 ratio of 15/100 ml/min (STP).

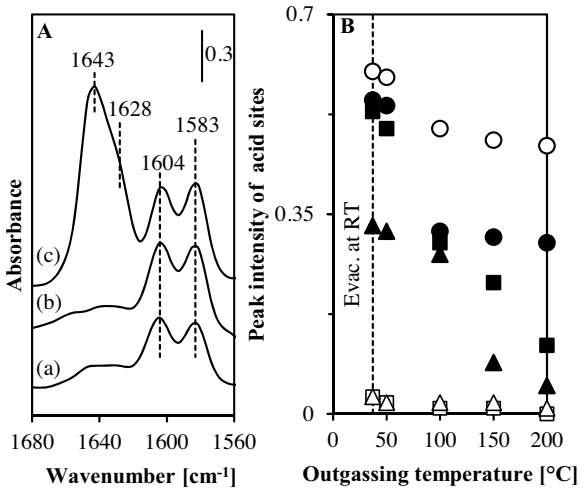

Fig. 4. (A) IR spectra of 2,6-lutidine adsorbed on (a) MSN, (b) Pt/MSN and (c) MoO_3/MSN at room temperature, followed by outgassing at 100 °C. (B) Variations of peak intensity at 1604 + 1583 cm^{-1} for MSN (▲), Pt/MSN (■) and MoO_3/MSN (●); and peak intensity at 1643 + 1628 cm^{-1} for MSN (△), Pt/MSN (□) and MoO_3/MSN (○) as a function of outgassing temperature after 2,6-lutidine adsorption.

the thermal cracking took place at and above 250 °C. The low activity of MSN was presumably due to the absence of the metallic-acid balance function, which should be in an appropriate amount for the composition of the *n*-heptane to be converted [39]. Similarly, Pt/MSN exhibited low activity in the isomerization of *n*-heptane, in which thermal cracking was observed at and above 200 °C, forming C_1 –C_6 products. However, trace amounts of *mono*- and *di*-branched isomers were observed at and above 200 °C. Therefore, it can be concluded that the MSN, MoO_3 and Pt/MSN were inefficient catalysts for *n*-heptane isomerization since the yield of isomers was less than 1% and the conversion rate of *n*-heptane was less than 1×10^{-9} mol/m^2s under either H_2 or N_2 carrier gas.

In contrast to the MSN, MoO_3 and Pt/MSN, MoO_3/MSN showed a substantial improvement in the activity, as the conversion rate of *n*-heptane over MoO_3/MSN was about thirtyfold higher than that on MSN or Pt/MSN. At and above 300 °C, the selectivity of *mono*-branched isomers (2-methylhexane, 3-methylhexane and 3-ethylpentane) reached more than 80% under hydrogen carrier gas. Besides, the formation of *di*-branched isomers simultaneously increased with the *n*-heptane conversion. At 300 °C, 6.4% selectivity of *di*-branched isomers was obtained with conversion rate of *n*-heptane of 26.74×10^{-9} mol/m^2s. The conversion rate and selectivity of *di*-branched isomers increased up to 31.66×10^{-9} mol/m^2s and 15.2% at 350 °C. However, almost no conversion of *n*-heptane was observed under nitrogen carrier gas, showing that almost no isomerization and/or thermal cracking was observed over MoO_3/MSN (Fig. 5). These results revealed that the presence of MoO_3 and H_2 was indispensable in the *n*-heptane isomerization on MSN catalyst. It was suggested that the high catalytic activity of MoO_3/MSN may be due to the presence of $(MoO_x)^-(H_y)^+$ formed from the interaction of MoO_3 and H_2 carrier gas [13]. As illustrated in Fig. 5, a significant drop in conversion rate was observed when the carrier gas was switched to nitrogen due to the gradual exhaustion of $(MoO_x)^-(H_y)^+$ acid sites on the surface of MoO_3/MSN. After the carrier gas was shifted back to hydrogen, the activity was gradually recovered. In addition, high activity and stability of MoO_3/MSN were observed for about 100 h at 350 °C in the presence of H_2 (Fig. 5). Previously, the promoting effect of hydrogen has been reported for several types of catalyst such as Zn-HBEA [4], CrO_3-ZrO_2 [39], and Zn/HZSM-5 [40], where the catalytic activities were observed only in the presence of hydrogen. Early report by Hattori and co-workers stated that the promotive effect of hydrogen can be defined by the generation of protonic acid sites, in which the formation of hydrogen migrates or spills over from noble metal sites onto the acidic oxide support, during the reaction [41–43]. Besides, this hydrogen spillover effect also has been observed by Iglesia and co-workers for zeolite supported metal catalysts [44,45].

Table 2 shows the comparison of the activity of MoO_3/MSN catalysts with MoO_3-loaded catalysts in *n*-heptane isomerization. Al-Kandari et al. reported the activity of *n*-heptane isomerization over MoO_3/TiO_2 catalyst in which the high selectivity towards *mono*-branched isomers (91.6%) was attributed to the balanced metal-acid in the $MoO_{2-x}(OH)_y$ phase [46]. The formation of acidic Mo-OH Brønsted was initialized by dissociation of hydrogen molecules into active hydrogen atoms by the metal, followed by bonding with surface oxygen atoms of MoO_2. However, no di-branched isomer was formed. Meanwhile, our research group has reported *n*-heptane isomerization over MoO_3-ZrO_2 and concluded that the activity of the catalyst was associated with the role of Lewis acid sites corresponding to the tetragonal phase of ZrO_2 [47]. Besides, *n*-heptane isomerization over MoO_3 catalysts associated with SiO_2 and Al_2O_3 has been studied by Alemán-Vázquez et al. who found that the MoO_xH_y acts as active phase in two bulk catalyst consist of 70 wt.% of MoO_3 and Al_2O_3 or SiO_2 binder [48]. Liu

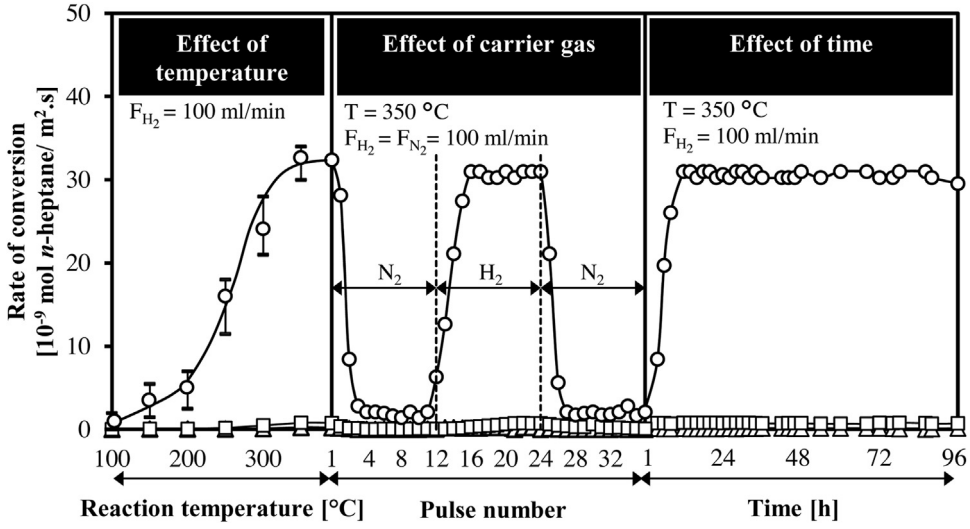

Fig. 5. Isomerization of *n*-heptane over MSN (△), Pt/MSN (□) and MoO_3/MSN (○). The data were taken from the average of the sixth, seventh and eighth pulses.

Table 2
Catalytic activity of catalysts for *n*-heptane isomerization.

Catalyst	Conversion [%]	Selectivity of isomers		Selectivity of cracking	Yield of isomers [%]	Reaction temperature [°C]	Reference
		Mono-branched	Multi-branched				
MoO_3/MSN	45	81.3	15.2	3.5	43.4	350	This study
MoO_3-TiO_2	46.7	91.6	–	8.4	42.7	300	[33]
MoO_3-ZrO_2	31	44.7	–	55.3	13.9	400	[34]
MoO_3/Al_2O_3	61.5	86.2	9.7	3.9	59	370	[35]
MoO_3/SiO_2	42.4	90.5	5.7	3.7	40.8	370	[35]
MoP/HBEA-40%	18	58.3	12.4	20.1	12.7	300	[36]

et al. reported that molybdenum phosphide supported on HBEA zeolite provided 18% conversion of *n*-heptane with 70.7% selectivity towards isomer products [49]. They suggested that an Mo of 40 wt.% was suitable to provide appropriate amount of metal for the hydrogenation–dehydrogenation process.

In this comparison, both MoO_3/MSN and MoO_3/ZrO_2 catalytic activity was conducted over pulse reactor while the other catalysts were tested by continuous flow reactor. However, the result obtained over the pulse reactor was comparable with the others since the measurement was taken as an average reading of pulses after the reaction was stable, at each reaction. In order to compare the activity of MoO_3/MSN, a single run in continuous reactor was conducted at optimum reaction temperature of 350 °C and the data is presented in Table 1. It was observed that the rate of conversion and yield of *mono* and *di*-branched isomers obtained over the continuous run was slightly low than the pulse reactor. This is might due to the equilibrium shifting of the *n*-heptane conversion towards isomers products in pulse reactor, leaving the hydrogen which escaped from the reaction phase by column effect [11]. In addition, the formation of coke after several pulses was prevented since there was a continuous flow of hydrogen as carrier gas which sustained the formation of active sites.

Based on the comparison results for *n*-heptane isomerization, it is suggested that MoO_3/MSN performed better than or comparably to than other supported MoO_3 catalysts in term of selectivity toward the formation of *mono*- and *di*-branched isomers. The high catalytic activity of the MoO_3/MSN is most probably due to the ability of the catalyst to form $(MoO_x)^-(H_y)^+$ in the presence of molecular hydrogen, despite the absence of noble metal. Similar phenomenon reported by Alemán-Vázquez et al. showed that the insertion of hydrogen atoms into the lattice of MoO_3 leads to the formation of MoO_xH_y, which consequently become the key step to generate the isomerization activity. It was reported that the formation of carbonaceous deposits was negligible under the experimental conditions of this work. The catalytic activity of the catalyst was mainly dependent on the acid properties of the catalyst, indicating that the presence of strong Brønsted acid sites in the fresh MoO_3 phase is important for a good activity of the catalyst in the hydroisomerization process. Besides, the intrinsic acidity of the Al_2O_3 or SiO_2 have an influence on the activity of the molybdenum trioxide as hydroisomerization catalyst [48].

Besides, the high surface area, large average pore diameter and presence of both intra- and inter-particle voids of the MSN support facilitated the dispersion of active Mo and transport of reactant and product molecules during the reaction. In addition, the existence of both intra- and inter-particle porosity in the MSN support also contributes to the formation of isomers products. The interparticle pores could facilitate the transport of the H_2 and reactant *n*-heptane as well as the products molecules during the catalytic reaction, leading to greater accessibility of active sites for the isomerization. Previously, Kitev et al. reported on the role of intercrystalline ordered mesopores for skeletal isomerization of 1-butene over FER zeolite [50]. It was suggested that the presence of interparticle pores in FER zeolite has improved the accessibility of the acid sites and the creation of new pore openings.

3.4. Dissociative-adsorption of hydrogen gas

Fig. 6 shows the IR spectra of 2,6-lutidine pre-adsorbed catalysts when heated in the presence of hydrogen gas from room temperature up to 250 °C. For MSN, the increase in the heating temperature in the presence of hydrogen gas did not alter the intensity of the absorbance bands at 1604 and 1583 cm^{-1}. This suggested that there is no interaction between MSN and hydrogen gas. Meanwhile, heating of 2,6-lutidine pre-adsorbed Pt/MSN in the presence of hydrogen gas slightly decreased the Lewis acid sites absorbance bands at 1606 and 1583 cm^{-1} with a concomitant increase of the absorbance bands at 1646 and 1629 cm^{-1}, which may be related to the formation of atomic hydrogen on the Pt surface (Pt-H) [51]. This result certified the ability of Pt in the dissociative-adsorption of molecular hydrogen to form atomic hydrogen at relatively low temperature. Although the formation of atomic hydrogen was observed on Pt/MSN, the promotive effect of atomic hydrogen in the *n*-heptane isomerization was not appreciable due to the inability of the electrically neutral charge of the silicate framework to hold active protonic acid sites.

The IR results of the interaction of hydrogen gas with MSN and Pt/MSN were in agreement with the ESR spectra in Fig. 7(A) and (B). Prior to the ESR measurement, the catalysts were outgassed at 400 °C for 1 h, followed by heating in the presence of hydrogen at elevated temperatures. All catalysts exhibited a small signal at $g = 1.99$, attributed to the trapped electrons or unpaired electrons, which were localized on metal cations and/or MSN support [52,53]. It was suggested that the trapped electron or unpaired electron was created due to desorption of hydroxyl groups from the surface catalysts, leaving electron-deficient metal cations. Heating of the catalysts in the presence of hydrogen gas up to 200 °C led to no significant change of the signals for MSN and Pt/MSN, indicating that no electrons were formed from hydrogen, which subsequently perturbed the electron-deficient metal cations. This also evidenced that no protons were formed on MSN and Pt/MSN, which finally led to the low activity of the MSN and Pt/MSN.

In contrast, the formation of acidic Brønsted in the form of $(MoO_x)^-(H_y)^+$ was clearly observed in the heating of 2,6-lutidine pre-adsorbed MoO_3/MSN under hydrogen gas (Fig. 6). As the heating temperature of MoO_3/MSN was raised up to 100 °C, the intensity of the absorbance bands at 1638 and 1631 cm^{-1}, corresponding to $(MoO_x)^-(H_y)^+$), gradually increased while the intensity of the absorbance bands at 1604 and 1583 cm^{-1}, corresponding to the Lewis acid sites, decreased. The extensive changes with the increasing temperature showed the dependence of the formation of $(MoO_x)^-(H_y)^+$) from molecular hydrogen on heating temperature.

The formation of active $(MoO_x)^-(H_y)^+$) in MoO_3/MSN was also evidenced indirectly by the formation of an electron in the ESR result in Fig. 7(C). The atomic hydrogen released an electron to form proton which subsequently bonded with an Mo atom to form

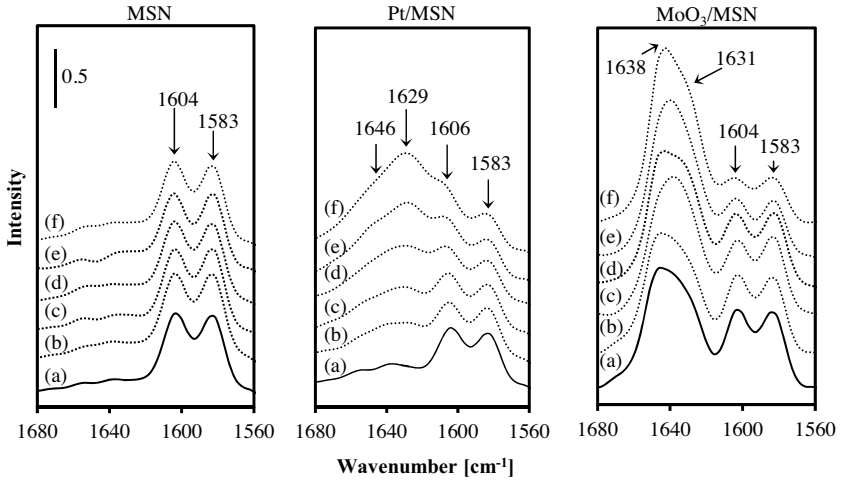

Fig. 6. IR spectral changes when 2,6-lutidine pre-adsorbed catalyst (a) was heated in hydrogen at (b) room temperature, (c) 50, (d) 100, (e) 150 and (f) 200 °C.

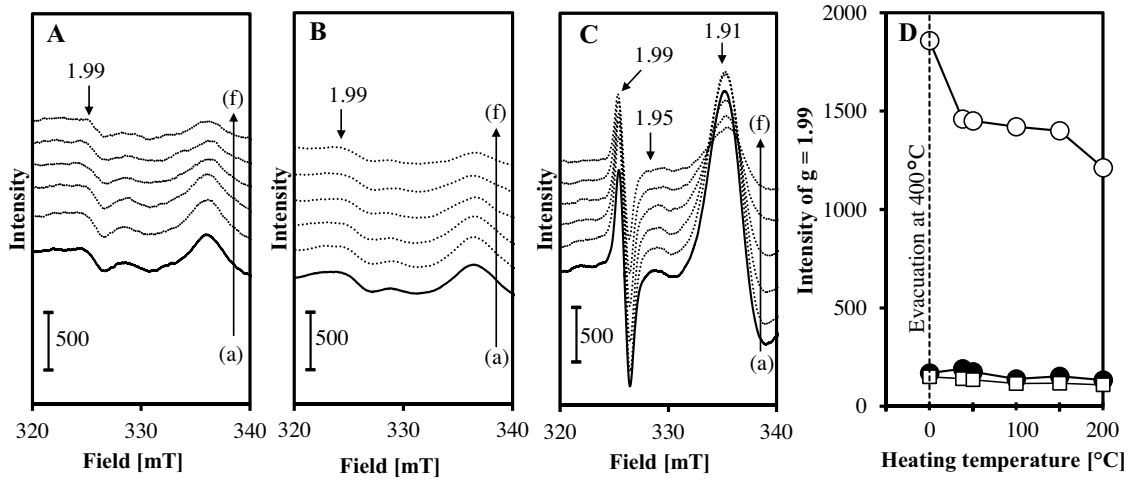

Fig. 7. ESR spectra of (A) MSN, (B) Pt/MSN and (C) MoO_3/MSN activated at (a) 400 °C for 1 h 100 Torr of hydrogen was adsorbed (b) room temperature, (c) 50, (d) 100, (e) 150 and (f) 200 °C. (D) Variations in the intensity of the ESR signal at g = 1.99 for MSN (□), Pt/MSN (●) and MoO_3/MSN (○) as a function of heating temperature. The dotted line represents the intensity of signals before the samples were heated in the presence of hydrogen.

$(MoO_x)^-(H_y)^+$), while the electron was trapped in the electron-deficient metal cations, resulting in the decrease of the ESR signal at g = 1.99. The changes of the signal at g = 1.99 are more clearly shown Fig. 7(D). The formation of electrons started to occur at 50 °C and the intensity of the signals was nearly restored to its original value at 200 °C, indicating that the unpaired electrons were fully occupied with the electrons formed from atomic hydrogen. In addition to the signal at g = 1.99, the MoO_3/MSN also exhibited another two signals at g = 1.91 and g = 1.95 which correspond to the tetra- and penta-coordinated Mo^{5+} species, respectively [43]. Heating of MoO_3/MSN in the presence of hydrogen did not change the signal at g = 1.95 but decreased the signal at g = 1.91. The result suggested that the tetra-coordinated MoO^{5+} species was involved in the formation of $(MoO_x)^-(H_y)^+$).

In the case of MoO_3/MSN, it is plausible that the MoO_3 metal acts as a specific active site for dissociative-adsorption of molecular hydrogen followed by the formation of acidic Brønsted. The Lewis acid sites played an important role in the stabilization of the acidic Brønsted by trapping the electrons. Previously, we have reported the role of acidic centers in the hydroisomerization of *n*-heptane over MoO_3 supported by ZrO_2, in which Lewis acidic centers corresponding to the tetragonal phase of ZrO_2 at 1595 + 1580 cm^{-1} were responsible for the high activity in *n*-heptane isomerization [47]. A previous study by Al-Kandari et al. reported that the balanced metal-acid in the $MoO_{2-x}(OH)_y$ is an active site for *n*-hexane and *n*-pentane isomerization [42]. Besides, the activity of Pt/MoO_3 has been reported to be associated with the formation of $(MoO_x)^-(H_y)^+$ [13].

4. Conclusion

Pt/MSN and MoO_3/MSN were prepared by physical mixing of Pt and MoO_3 with MSN for isomerization of *n*-heptane. XRD and N_2 physisorption results indicated that the introduction of Pt did not change the MSN much, whereas the introduction of MoO_3 significantly altered the surface area and average pore diameter of MSN. In addition, the IR result revealed that the formation of new absorbance bands at 3600, 3569 and 3520 cm^{-1} corresponded to the stretching of the structural environment of OH and perturbed hydroxyl groups due to the presence of Mo, which interacted with the lattice structure of MSN. 2,6-Lutidine adsorbed IR spectra of MoO_3/MSN revealed the presence of doublet bands at 1604 and 1583 cm^{-1}, which could be attributed to Lewis acid sites and another doublet bands at 1638 and 1631 cm^{-1} attributed to for Brønsted acid sites after outgassing at and below 150 °C showing the presence of medium and strong acidic sites. However, almost

no Brønsted acid sites and only a small number of Lewis acid site were observed for both MSN and Pt/MSN.

MSN, MoO_3 and Pt/MSN showed low activity in *n*-heptane isomerization in the presence of hydrogen or nitrogen carrier gas due to the inability of the catalysts to form active protonic acid sites to initiate the isomerization. Meanwhile, the presence of MoO_3 markedly enhanced the catalytic activity of MSN in *n*-heptane isomerization in the presence of hydrogen carrier gas. At 350 °C, the yield of *mono*- and *di*-branched isomers reached 36.6 and 6.8%. The high activity of MoO_3/MSN was supported by hydrogen adsorbed IR and ESR studies in which the interaction of MoO_3 and hydrogen gas formed $(MoO_x)^-(H_y)^+$ active sites for *n*-heptane isomerization. In fact, no activity was observed on MoO_3/MSN in the presence of nitrogen carrier gas. The results of the study showed the potential of MoO_3/MSN for hydrocracking, alkylation and/or other general solid acid-catalyzed reactions.

Acknowledgements

This work was supported by the Universiti Teknologi Malaysia through Research University Grant no. 00M67. Our gratitude also goes to the Ministry of Higher Education (MOHE) Malaysia for the award of MyPhD Scholarship (Nor Aiza Abdul Fatah).

References

[1] R. Yadav, A. Sakthivel, Appl. Catal. A 481 (2014) 143–160.
[2] A.K. Singh, R. Yadav, V. Sudarsan, K. Kishore, S. Upadhyayula, A. Sakthivel, RSC Adv. 4 (2014) 8727–8734.
[3] S. Triwahyono, Z. Abdullah, A.A. Jalil, J. Nat. Gas Chem. 15 (2006) 247–252.
[4] N.H.N. Kamarudin, A.A. Jalil, S. Triwahyono, R.R. Mukti, M.A.A. Aziz, H.D. Setiabudi, M.N.M. Muhid, H. Hamdan, Appl. Catal. A 431 (2012) 104–112.
[5] T. Kusakari, K. Tomoshige, K. Fujimoto, Appl. Catal. A 224 (2002) 219–228.
[6] A. Chica, A. Corma, P.J. Miguel, Catal. Today 65 (2001) 101–110.
[7] S.M. Sidik, A.A. Jalil, S. Triwahyono, T.A.T. Abdullah, A. Ripin, RSC Adv. 5 (2015) 37405–37414.
[8] M.A.A. Aziz, A.A. Jalil, S. Triwahyono, R.R. Mukhti, Y.H. Taufiq-Yap, M.R. Sazegar, Appl. Catal. B 147 (2014) 359–368.
[9] N.H.N. Kamarudin, A.A. Jalil, S. Triwahyono, N.F.M. Salleh, A.H. Karim, R.R. Mukhti, B.H. Hameed, A. Ahmad, Microporous Mesoporous Mater. 180 (2013) 235–241.
[10] A.H. Karim, A.A. Jalil, S. Triwahyono, S.M. Sidik, N.H.N. Kamarudin, R. Jusoh, N.W.C. Jusoh, B.H. Hameed, J. Colloid Interface Sci. 386 (2012) 307–314.
[11] M.R. Sazegar, A.A. Jalil, S. Triwahyono, R.R. Mukti, M. Aziz, M.A.A. Aziz, H.D. Setiabudi, N.H.N. Kamarudin, Chem. Eng. J. 240 (2014) 352–361.
[12] H. Sakagami, T. Ohno, H. Itoh, Z. Li, N. Takahashi, T. Matsuda, Appl. Catal. A 470 (2014) 8–14.
[13] S.N. Timmiati, A.A. Jalil, S. Triwahyono, H.D. Setiabudi, N.H.R. Annuar, Appl. Catal. A 459 (2013) 8–16.
[14] P.D. Gallo, C. Pham-Huu, C. Bouchy, C. Estournes, M.J. Ledoux, Appl. Catal. A 156 (1997) 131–149.
[15] T. Matsuda, T. Ohno, Y. Hiramatsu, Z. Li, H. Sakagami, N. Takahashi, App. Catal. A 362 (2009) 40–46.
[16] H. Nair, J.E. Gatt, J.T. Miller, C.D. Baertsch, J. Catal. 279 (2011) 144–154.
[17] D.P. Debecker, B. Schimmoeller, M. Stoyanova, C. Poleunis, P. Bertrand, U. Rodemerck, E.M. Gaigneaux, J. Catal. 277 (2011) 154–163.
[18] Y.M. Wang, Z.Y. Wu, H.J. Wang, J.H. Zhu, Adv. Funct. Mater. 16 (2006) 2374–2386.
[19] S.-C. Shen, S. Kawi, Appl. Catal. B 45 (2003) 63–76.
[20] A.K. Medina-Mendoza, M.A. Cortés-Jácome, J.A. Toledo-Antonio, C. Angeles-Chávez, E. López-Salinas, I. Cuauhtémoc-López, M.C. Barrera, J. Escobar, J. Navarrete, I. Hernández, App. Catal. B 106 (2011) 14–25.
[21] K.V.R. Chary, K.R. Reddy, G. Kishan, J.W. Niemantsverdriet, G. Mestl, J. Catal. 226 (2004) 283–291.
[22] B. Wang, G. Ding, Y. Shang, J. Lv, H. Wang, E. Wang, Z. Li, X. Ma, S. Qin, Q. Sun, Appl. Catal. A 431 (2012) 144–150.
[23] P. Arnoldy, J.C.M. de Jonge, J.A. Moulijn, J. Phys. Chem. 89 (1985) 4517–4526.
[24] L.P. Singh, S.K. Agarwal, S.K. Bhattacharyya, U. Sharma, S. Ahalawat, Nanomater. Nanotech. 1 (2011) 44–51.
[25] G.S. Zakharova, C. Taschner, V.L. Volkov, I. Hellman, R. Klingeler, A. Leonhardt, B. Buchner, Solid. State Sci. 9 (2007) 1028–1032.
[26] T. Ivanova, M. Surtchev, K. Gesheva, Mater. Lett. 53 (2002) 250–257.
[27] A. Kierys, S. Pasieczna-Patkowska, J. Ryczkowski, A. Boríowka, J. Goworek, Eur. Phys. J. Special Topics 154 (2008) 335–338.
[28] D. Dombrowski, J. Hoffmann, J. Fruwert, T. Stock, J. Chem. Soc. Faraday Trans. 1 81 (1985) 2257–2271.
[29] A. Jentys, J.A. Lercher, Stud. Surf. Sci. Catal. 137 (2001) 345–386.
[30] H.D. Setiabudi, A.A. Jalil, S. Triwahyono, N.H.N. Kamarudin, R.R. Mukti, Appl. Catal. A 417 (2012) 190–199.
[31] Z. Li, L. Gao, S. Zheng, Appl. Catal. A 236 (2002) 163–171.
[32] A. Guevara-Lara, A.E. Cruz-Pérez, Z. Contreras-Valdez, J. Mogica-Betancourt, A. Alvarez-Hernández, M. Vrinat, Catal. Today 149 (2010) 288–294.
[33] N.W.C. Jusoh, A.A. Jalil, S. Triwahyono, H.D. Setiabudi, N. Sapawe, M.A.H. Satar, A.H. Karim, N.H.N. Kamarudin, R. Jusoh, N.F. Jaafar, N. Salamun, J. Efendi, App. Catal. A 468 (2013) 276–287.
[34] S.J. Gregg, Adsorption, Surface Area and Porosity, Academic Press, London, UK, 1982.
[35] E. Ghedini, F. Menegazzo, M. Signoretto, M. Manzoli, F. Pinna, G. Strukul, J. Catal. 273 (2010) 266–273.
[36] V. Lebarbier, G. Clet, M. Houalla, J. Phys. Chem. B 110 (2006) 22608–22617.
[37] S. Al-Kandari, H. Al-Kandari, A.M. Mohamed, F. Al-Kharafi, A. Katrib, Appl. Catal. A 475 (2014) 497–502.
[38] F. Regali, L.F. Liotta, A.M. Venezia, M. Boutonnet, S. Järås, App. Catal. A 469 (2014) 328–339.
[39] N.H.R. Annuar, A.A. Jalil, S. Triwahyono, Z. Ramli, J. Mol. Catal. 377 (2013) 162–172.
[40] S. Triwahyono, A.A. Jalil, M. Musthofa, App. Catal. A 372 (2010) 90–93.
[41] H. Hattori, Stud. Surf. Sci. Catal. 138 (2001) 3–12.
[42] S. Triwahyono, T. Yamada, H. Hattori, App. Catal. A 250 (2003) 65–73.
[43] S. Triwahyono, T. Yamada, H. Hattori, App. Catal. A 250 (2003) 75–81.
[44] J.A. Biscardi, E. Iglesia, Catal. Today 31 (1996) 207–231.
[45] E. Iglesia, D.G. Barton, J.A. Biscardi, M.J.L. Gines, S.L. Soled, Catal. Today 38 (1997) 339–360.
[46] H. Al-Kandari, A.M. Mohamed, F. Al-Kharafi, M.I. Zaki, A. Katrib, App. Catal. A 417 (2012) 298–305.
[47] N.N. Ruslan, N.A. Fadzlillah, A.H. Karim, A.A. Jalil, S. Triwahyono, Appl. Catal. A 406 (2011) 102–112.
[48] L.O. Alemán-Vázquez, F. Hernández-Pérez, J.L. Cano-Domínguez, A. Rodríguez-Hernández, J.L. García-Gutiérrez, Fuel 117 (2014) 463–469.
[49] P. Liu, W.T. Chang, J. Wang, M.Y. Wu, Y.X. Li, Catal. Commun. 66 (2015) 79–82.
[50] Yu. P. Khitev, I.I. Ivanova, Yu G. Kolyagin, O.A. Ponomareva, Appl. Catal. A 441 (2012) 124–135.
[51] R.R. Xu, Z. Gao, Y. Xu, Progress in Zeolite Science: A China Perspectives, World Scientific, Singapore, 1995, pp. 60.
[52] H.D. Setiabudi, A.A. Jalil, S. Triwahyono, J. Catal. 294 (2012) 128–135.
[53] R. Macdonald, R.F. Howe, X. Zhang, W. Zhou, J. Photochem. Photobiol. A 216 (2010) 238–243.